Optical Magnetization, Part III: Theory of molecular magneto-electric rectification

ELIZABETH F. C. DREYER,[1,*] ALEXANDER A. FISHER,[1,2] GREGORY SMAIL,[1,2] PETR ANISIMOV,[3] AND STEPHEN C. RAND[1,2]

[1]*Center for Dynamic Magneto-Optics, Dept. of Electrical Engineering & Computer Science University of Michigan, Ann Arbor, MI 48109-2099, USA*
[2]*Division of Applied Physics, University of Michigan, Ann Arbor, MI 48109, USA*
[3]*Los Alamos National Laboratory, Los Alamos, NM 87545*
[*]*efcloos@umich.edu*

Abstract: A fully quantized analysis is presented of induced magneto-electric rectification in individual diatomic molecules in the steady-state regime. Good agreement is obtained between this quantum theory and a classical model that includes the same key kinematic elements but predicts temporal dynamics as well. At the molecular level, an enhanced magneto-electric optical interaction driven by dual optical fields E and H^* is shown to give rise to a static electric dipole (ED) moment oriented along the propagation direction of linearly-polarized light in dielectric materials. This longitudinal Hall effect or "charge separation" interaction is quadratic with respect to the incident field strength and exhibits an induced moment that is limited by the ED transition moment of the molecular resonance. Overall, the two-photon dynamics can be described as first establishing an electric polarization and imparting orbital angular momentum on which the magnetic field exerts torque in the excited state of the molecule. Magnetic torque mediates an exchange of orbital and rotational angular momenta that de-excites the molecule and simultaneously enhances magneto-electric rectification. Material properties that affect magneto-electric response at the molecular level are identified.

OCIS codes: (190.0190) Nonlinear optics; (190.4410) Nonlinear optics, parametric processes; (190.7710) Ultrafast nonlinear optics; (320.7110) Ultrafast nonlinear optics; (350.3618) Left-handed materials.

References and links

1. J. C. Ginn, I. Brener, D. W. Peters, J. R. Wendt, J. O. Stevens, P. F. Hines, L. I. Basilio, L. K. Warne, J. F. Ihlefeld, P. G. Clem, and M. B. Sinclair, "Realizing optical magnetism from dielectric metamaterials," Phys. Rev. Lett. **108**, 097402 (2012).
2. W. F. Koehl, B. B. Buckley, F. J. Heremans, G. Calusine, and D. D. Awschalom, "Room temperature coherent control of defect spin qubits in silicon carbide," Nature **479**, 84 (2011).
3. G. D. Fuchs, G. Burkard, P. V. Klimov, and D. D. Awschalom, "A quantum memory intrinsic to single nitrogen–vacancy centres in diamond," Nat. Phys. **7**, 789 (2011).
4. C. D. Stanciu, F. Hansteen, A. V. Kimel, A. Kirilyuk, A. Tsukamoto, A. Itoh, and Th. Rasing, "All-optical magnetic recording with circularly polarized pulses," Phys. Rev. Lett. **99**, 047601 (2007).
5. W.M. Fisher and S.C. Rand, "Optically-induced charge separation and terahertz emission in unbiased dielectrics," J. Appl. Phys. **109**, 064903 (2011).
6. S. L. Oliveira, S. C. Rand, "Intense nonlinear magnetic dipole radiation at optical frequencies: Molecular scattering in a dielectric liquid," Phys. Rev. Lett. **98**, 093901 (2007).
7. S. C. Rand, W. M. Fisher, S. L. Oliveira, "Optically-induced magnetization in homogeneous, undoped dielectric media," *J.O.S.A. B* **25**, 1106 (2008); Erratum J.O.S.A. B **26**, 1549 (2009).
8. W. M. Fisher and S. C. Rand, "Dependence of optical magnetic response on molecular electronic structure," J. Lumin. **129**, 1407 (2009).
9. K. Y. Bliokh, Y.S. Kivshar, and F. Nori, "Magnetoelectric effects in local light-matter interactions," Phys. Rev. Lett. **113**, 033601 (2014).
10. A. Einstein, W. J. de Haas, "Experimenteller nachweis der ampereschen molekularströme," Deut. Phys. Ges., Verhandlungen **17**, pp. 152–170 (1915).
11. S. Boettcher and C.M. Bender, "Real spectra in non-hermitian Hamiltonians having PT symmetry," Phys. Rev. Lett. **80**, 5243-5246 (1998).

12. A. A. Fisher, E. F. C. Dreyer, A. Chakrabarty and S. C. Rand, "Optical magnetization, Part I: Experiments on radiant optical magnetization in solids," Opt. Express **24**, No. 23 26064 (2016).
13. A. A. Fisher, E. F. C. Dreyer, A. Chakrabarty and S. C. Rand, "Optical magnetization, Part II: Theory of induced optical magnetism," Opt. Express **24**, No. 23 26055 (2016).
14. N. A. Spaldin and M. Fiebig, "The renaissance of magnetoelectric multiferroics," Science **309**, 391-392 (2005).
15. A. A. Fisher, E. F. Cloos, W. M. Fisher, and S. C. Rand, "Dynamic symmetry-breaking in a simple quantum model of magneto-electric rectification, magnetization, and harmonic generation," Opt. Express **22**, 2910 (2014).
16. V.O. Deutschbein, "Experimentelle untersuchungen uber die vorgange bei der lichtemission," Ann. Phys. Vol. 5, No. **36** 183 (1939).
17. M. Kasperczyk, S. Person, D. Ananias, L.D. Carlos, and L. Novotny, "Excitation of magnetic dipole transitions at optical frequencies," Phys. Rev. Lett. **114**, 163903 (2015).
18. N.R. Brewer, Z.N. Buckholtz, Z.J. Simmons, E.A. Mueller, and D.D. Yavuz, "Coherent magnetic response at optical frequencies using atomic transitions," Phys. Rev. X **7**, 011005 (2017).
19. See for example E. Hecht, *Optics*, Third edition (Addison Wesley Longman, 1998), pp. 69.
20. See for example G.R. Fowles, *Analytic Mechanics* (Holt Rinehart and Winston, 1962), pp. 206.
21. A. Fisher, "Experiments and theory of induced optical magnetization," Ph. D. dissertation, University of Michigan, 2016, p. 27 and p. 123.
22. W.M. Fisher and S.C. Rand, "Light-induced dynamics in the Lorentz oscillator model with magnetic forces," Phys. Rev. A **82**, 013802 (2010).
23. G. Herzberg, *Spectra of Diatomic Molecules*, Second edition (Van Nostrand Reinhold, 1950), p. 129.
24. C. Cohen-Tannoudji and S. Reynaud, Dressed Atom Approach to resonance fluorescence, in *Multiphoton Processes*, eds. J. Eberly and P. Lambropoulos (J. Wiley & Sons, 1977), pp. 103-118.
25. A. Lou, E.F.C. Dreyer, T. Marks, and S.C. Rand, "Design principles for magneto-electric materials: All-electric susceptibilities relevant to optimal molecular chromophores," J. Phys. Chem. C **121**(30), 16491-16500 (2017).

1. Introduction

Optical interactions mediated by the magnetic field of light are potentially relevant to many fields including metamaterials, spintronics, quantum information, and data storage. In recent years novel applications of electromagnetism have emerged from the search for negative permeability in structured materials [1], coherent optical spin control of semiconductor charge carriers [2] or luminescent centers [3], and ultrafast switching of magnetic domains [4]. As a consequence, any prospect of eliciting response from homogeneous materials using novel nonlinear processes reliant on the optical magnetic field could accelerate the development of unforeseen magneto-photonic technologies. The realization of strong optical magnetism in nominally "non-magnetic" media for example could lead to novel forms of light-by-light switching, energy conversion, negative permeability in natural materials or the generation of large (oscillatory) magnetic fields without current-carrying coils [5-8]. In this paper, a dual field magneto-electric (M-E) optical process is shown to induce a strong rectification field at the molecular level [9] through a mechanism that is somewhat reminiscent of the Einstein-de Haas effect [10]. Optical excitation deposits orbital angular momentum in the molecules and magnetic torque converts it to molecular rotation. During this process a static longitudinal electric dipole (ED) moment is induced that can be as large as the electric dipole transition moment. A detailed quantum model is formulated, as well as a corresponding classical model that has the advantage of permitting predictions of system dynamics that are not possible with the steady-state quantum analysis. The magneto-electric process is shown to be universally allowed at the molecular level, despite the fact it is second-order with respect to the incident field. This is a result of PT-symmetry that governs the interaction [see [11] and Appendix A]. Predictions of transient response are made and related to the experimental and theoretical results for magneto-electric optical magnetization presented in earlier papers [12, 13].

Magneto-electric phenomena have been investigated at the macroscopic level in solids for some time [14] but at the microscopic level have only been reported in light scattering experiments [12] and analyzed [13,15] comparatively recently. Bulk M-E materials typically include magnetic constituents that enable the generation of electric voltages via

magnetostriction or they make use of electric fields to control magnetic domains. In contrast to this, here we analyze the dynamics of a non-magnetic, 2-level model that produces a rectification polarization $P^{(2)}(0)$ via a second-order nonlinearity driven jointly by the electric and magnetic field components of light in individual molecules. Surprisingly, no special crystal symmetry is necessary to support this magneto-electric interaction, although M-E charge separation can be enhanced following guidelines for molecular design developed in this paper. In *atoms* magnetic transitions at optical frequencies typically require a circularly-polarized electric field [16], though oriented optical magnetic fields can be used to drive magnetic dipole transitions in rare earth ions [17, 18]. Generally, in spinless, low-Z atoms irradiated with linearly-polarized light, the high frequency of the optical magnetic field does not match the low frequency range of transitions between (degenerate or nearly-degenerate) excited state sublevels. However, in *molecular* media very strong magnetic effects can take place as the result of magnetic torque dynamics [13] that unexpectedly make optical magnetic resonance possible at elevated field strengths.

In this paper a quantum treatment of M-E rectification is developed to furnish a closed form, steady-state solution for $P^{(2)}(0)$. A simple classical model based on the same dynamic elements is also formulated to enable predictions of temporal dynamics. Because the rectification nonlinearity is strongly coupled with optical magnetization, some results are shown for the induced magnetic moment, although similar results have been described previously [13]. Magneto-electric rectification is shown to induce a static longitudinal electric dipole in the medium whose magnitude at high intensities exceeds that of the first-order electric polarization giving rise to Rayleigh scattering. Large transition moments and low rotation frequencies are found to strengthen magneto-electric response. Calculations of transient behavior reveal that the response evolves from under- to over-damped as the librational relaxation rate is increased, and instabilities appear under conditions of low damping or very high field strengths. Finally, the intensity required to reach maximum rectification field strength is found to scale inversely with the rotation/libration frequency of the molecule.

2. A classical model for magneto-electric response

Quantum mechanical dynamics can sometimes be visualized with classical analysis when excited states play a minor role in determining the optical response of a system. Here we adopt this perspective to anticipate the role of torque exerted by the optical magnetic field in magneto-electric interactions at the molecular level, the quantum version of which is covered in Section 3. An intuitive picture of the key dynamics of such interactions is thereby provided before the formal quantum theory is introduced, and a computational approach is outlined whereby temporal dynamics of M-E interactions can be simulated.

The conventional classical model that relates the optical properties of a medium to charge dynamics on the atomic scale depicts an electron as a small mass attached to a nucleus by a mechanical spring. Motion of the electron subject to an electric field is determined by classical equations of motion referenced to a stationary equilibrium point chosen to be the origin [19]. Here we extend the customary model to include the Lorentz force on molecules which are allowed to rotate. In this case, the equilibrium point of the electron undergoes rotational motion and cannot be used as a fixed point of reference. Instead the origin of the coordinate system in the present analysis is chosen to coincide with the center-of-mass of the molecule. This introduces a new degree of freedom, namely rotation about the center-of mass, which permits the optical magnetic field to exert torque on the molecular charge system to alter the axis along which angular momentum is aligned.

The displacement of the electron from equilibrium is taken to be $\bar{r} = \bar{\xi} - \bar{r}_A$, where $\bar{r}_A$ specifies the point of equilibrium. This designates the point of attachment of the electron on

its spring in the classical picture shown in Fig. 1, whereas $\bar{\xi}$ specifies electron position with respect to the center-of-mass. The applied fields cause displacements and librations of the electron about the point of equilibrium. Hence the equation of motion with respect to the center-of-mass in a fixed molecular frame of reference is

$$\frac{d^2\bar{\xi}(t)}{dt^2} + \gamma\frac{d\bar{\xi}(t)}{dt} + \omega_0^2(\bar{\xi}(t) - \bar{r}_A) = \frac{\bar{F}(t)}{m}. \tag{2.1}$$

Here ω_0 and γ are the resonant frequency and damping constants of the Hooke's Law oscillator, and *m* is the electron effective mass. $\bar{F}(t)$ is the external force acting on the oscillator. It has the form

$$\bar{F}(t) = q(\bar{E} + \bar{\mathrm{v}} \times \bar{B}), \tag{2.2}$$

where q is the charge, $\bar{E}$ and $\bar{B}$ are the applied fields oriented along *x* and *y* respectively, and $\bar{\mathrm{v}}$ is velocity.

In Eq. (2.1), the internal restoring force experienced by the electron has been written as $\bar{F}_i(t) = -m\omega_0^2\bar{r}(t)$. Whenever the electron is out of equilibrium, the molecule experiences an equal but opposite reaction force $\bar{F}_r = -\bar{F}_i$, applied to the point of equilibrium. That is, the electron exerts a torque on the molecule given by

$$\bar{T} = \bar{r}_A \times (m\omega_0^2\bar{r}) = m\omega_0^2\bar{r}_A \times \bar{\xi}\ . \tag{2.3}$$

This torque modifies the components of angular velocity in a fashion that depends on the moment of inertia about each Cartesian axis. For a homonuclear diatomic molecule there are two distinct moments of inertia denoted by

$$I_\perp \equiv I_y = I_z, \tag{2.4}$$

$$I_{//} \equiv I_x. \tag{2.5}$$

The torque due to the reaction force is therefore capable of creating components of angular velocity in all three directions [20] according to

$$I_{//}\frac{d\Omega_x}{dt} = T_x, \tag{2.6}$$

$$I_\perp\frac{d\Omega_y}{dt} = T_y, \tag{2.7}$$

$$I_\perp\frac{d\Omega_z}{dt} = T_z. \tag{2.8}$$

Note that for the specific initial condition $\bar{r}_A(0) = r_A\hat{y}$, the torque in Eq. (2.3) develops components only along $\hat{x}$ and $\hat{z}$, since $\bar{r}_A \times \bar{\xi}$ in Eq. (2.3) has no components along $\hat{y}$. That is, $T_y(0) = 0$. According to Eqs. (2.6) and (2.8), the non-vanishing torque components in this case alter linear velocities in the *y-z* and *x-y* planes as time progresses. Motion is therefore inherently three-dimensional in the model. The same conclusion is reached for an initial

condition of $\bar{r}_A(0) = r_A\hat{z}$. However, for an initial condition $\bar{r}_A(0) = r_A\hat{x}$, corresponding to a point of equilibrium located on the axis of the molecule, torque has no effect on the dynamics since $\bar{r}_A(0) \times \bar{\xi}(0) = 0$. Consequently, to investigate the role of torque in this model, all calculations were performed using the initial condition $\bar{r}_A(0) = r_A\hat{y}$.

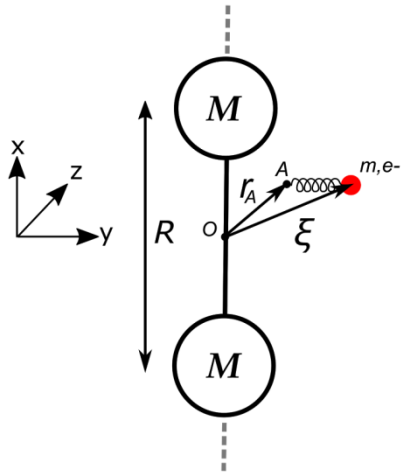

Fig. 1. Model of a homonuclear diatomic molecule, together with the coordinate system and position vectors $\bar{\xi}$ and $\bar{r}_A$ specifying electron position and point of equilibrium respectively.

In general, the exertion of torque by the displaced electron causes the molecule to rotate. In the reference frame of the molecule, this changes the position of the equilibrium or attachment point, as described by the equation

$$\frac{d\bar{r}_A(t)}{dt} = \bar{\Omega}(t) \times \bar{r}_A(t), \tag{2.9}$$

where $\bar{\Omega}(t)$ is the angular velocity of the molecule.

The quantities of main interest here are the instantaneous values of the induced electric polarization $\bar{P}(t)$ at zero frequency and the optical magnetization $\bar{M}(t)$. Their definitions in terms of the given coordinate system are

$$\bar{P}(t) = e\bar{\xi}(t), \tag{2.10}$$

and

$$\bar{M}(t) = -\frac{e}{2m}\bar{L} = -\frac{e}{2}\bar{\xi}(t) \times \frac{d\bar{\xi}(t)}{dt}. \tag{2.11}$$

These quantities were simulated by applying finite time steps in a Matlab code that integrated Eq. (2.1). For the *n*th iteration, electron position $\bar{\xi}(t_{n+1})$ was calculated from $\bar{\xi}(t_n)$ and inserted into Eq. (2.3) to update torque components. Angular velocities from Eqs. (2.6-2.8) were then similarly used to obtain the change in the "tether" position, $\Delta\bar{r}_A(t_n)$, from Eq. (2.9). This yielded a new value of $\bar{r}_A$, given by $\bar{r}_A(t_{n+1}) = \bar{r}_A(t_n) + \Delta\bar{r}_A(t_n)$, to be inserted into Eq. (2.1) and the procedure was iterated.

The results are plotted in Figs. 2 and 3 to illustrate several features of a *molecular*, as opposed to an *atomic*, model of magneto-electric dynamics. The magnitudes and temporal dynamics of *P(t)* and *M(t)* are seen to depend on moments of inertia, applied torque, and internal damping. For example, in these two figures, the moments of inertia $I_{//}$ and $I_{\perp}$ have been assigned arbitrary but representative values that are inversely proportional to optical and rotation frequencies of the molecule respectively. By comparing left and right plots in Fig. 2 the average displacement of the electron away from its initial equilibrium point is seen to increase roughly a thousand-fold when $I_{\perp} / I_{//}$ is increased from a value of 1 to 1000. In Fig. 3, magnetization is enhanced by a similar factor as the result of varying this structural ratio. The enhancement results from a large increase in the effective area enclosed by librational motion of the electron when the rotation axis is altered by the action of magnetic torque.

In Fig. 2 (and Fig. 4) fast oscillations at the second harmonic of the optical frequency accompany the formation of the static electric dipole moment along the propagation axis. However the harmonic motion does not experience dynamic enhancement, does not radiate, and does not contribute to the average offset polarization which is the rectification or "charge separation" signal. Hence it will be ignored here. The magnetization on the other hand is radiant. This is because it is driven by the optical magnetic field which breaks any centrosymmetry which may be present, it is transverse to the propagation axis, and it oscillates at the fundamental frequency (Fig. 3). Figure 4 shows that an increase of librational damping removes the long-period nutation transients (Rabi oscillations) while not affecting the asymptotic values of rectification or magnetization. This is the same behavior expected of nutation in all-electric interactions.

Figure 5 shows that the charge separation and magnetization both reach peak values at shorter times for elevated field strengths in under-damped conditions. Stronger driving fields force faster response. In this figure the rectification and magnetization responses show signs of the onset of saturation however, since the rectification increases less than the magnetization between low and high fields. This is because the former is a second-order process while the latter is third-order in a classical treatment. For the simulations of Figs. 2-6, magnetization and polarization are plotted in the same units for direct comparison, as P and M/c. Some parameters were assigned fixed values such as $\omega_0 = 1.63\times10^{16}$ *rad/s*, $I_{//} = \hbar / \omega_0$, and $\omega = 0.9\omega_0$. Values for other quantities are provided in the figure captions. The product of electron charge with the steady-state limit of the tether position r_A had a value of 2.4×10^{-30} *C.m*. This is equivalent to a quantum mechanical ED transition moment in a hydrogenic model [21] of $\mu_e = 1.26\times10^{-30}\, C\cdot m$. It may then be noted that, as expected, the oscillations in Figs. 4(a) and 5(b) which have periods of 0.32 and 0.21 ps are in quite good agreement with inverse Rabi frequencies of 0.26 and 0.18 ps defined by $\nu_R^{-1} \equiv (\mu_e E / h)^{-1}$.

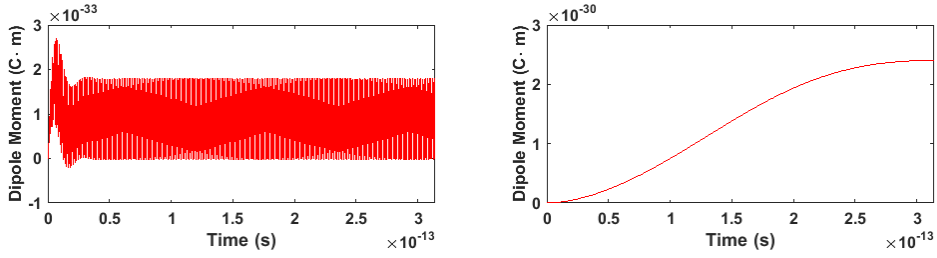

Fig. 2. Evolution of charge separation, $P_z(0)$, of the test charge versus time for $I_\perp / I_{//} = 1$ (left) and $I_\perp / I_{//} = 1000$ (right). Other fixed parameters were $E = 1 \times 10^9 V/m$ and $\gamma = 0.1\omega_0$.

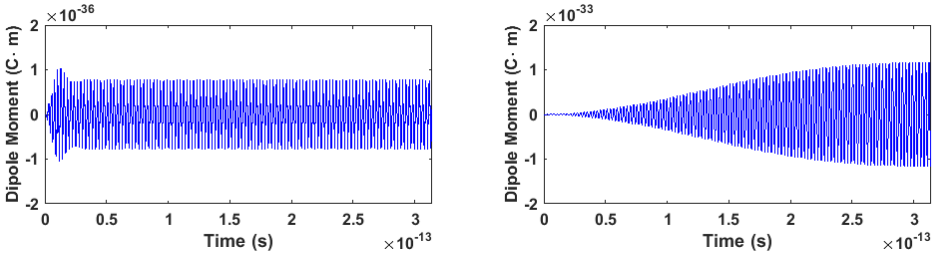

Fig. 3. Evolution of the magnetic moment (divided by c) versus time for $I_\perp / I_{//} = 1$ (left) and $I_\perp / I_{//} = 1000$ (right). Other fixed parameters were $E = 1 \times 10^9 V/m$ and $\gamma = 0.1\omega_0$.

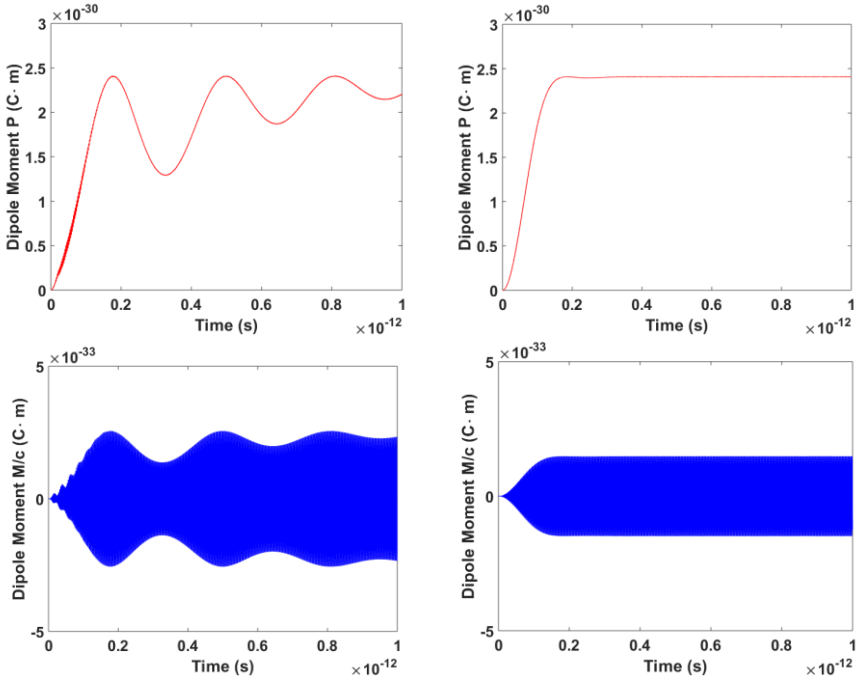

Fig. 4. Evolution of charge separation (top) and magnetization/c (bottom) versus time for different values of the magnetic (librational) damping coefficients: $\gamma = 0.03\omega_0$ (left) and $\gamma = 0.3\omega_0$ (right). Other fixed parameters were $E = 2 \times 10^9 V/m$ and $I_\perp / I_{//} = 1000$.

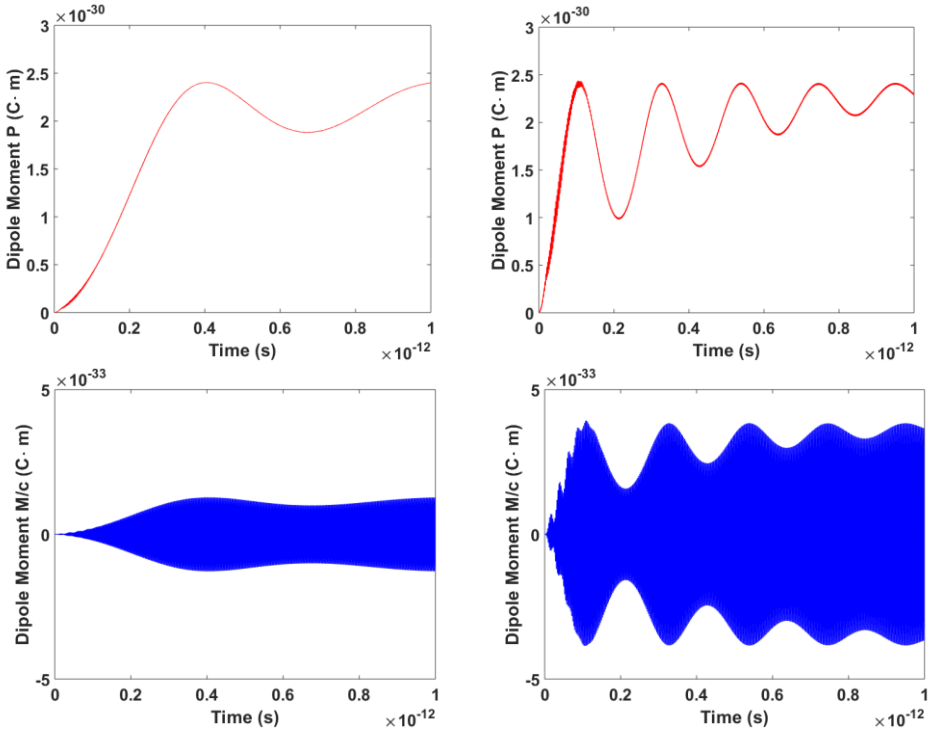

Fig. 5. Evolution of charge separation (top) and magnetization/c (bottom) versus time for different values of the applied electric field. The electric field strength is $E = 10^9 V/m$ (left) and $E = 3\times10^9 V/m$ (right). Other fixed parameters were $I_\perp / I_{//} = 1000$ and $\gamma = 0.03\omega_0$.

At elevated field strengths, instabilities appeared in the temporal evolution of the system. This emphasized the sensitivity of the extended Drude-Lorentz model to parametric instabilities, arising from inclusion of the magnetic Lorentz force [22]. Figure 6 shows traces of the electric and magnetic moments versus time at high optical field strength, with and without strong librational damping. Self-pulsing and frequency-chirped oscillations which are not at the Rabi frequency are evident in the traces.

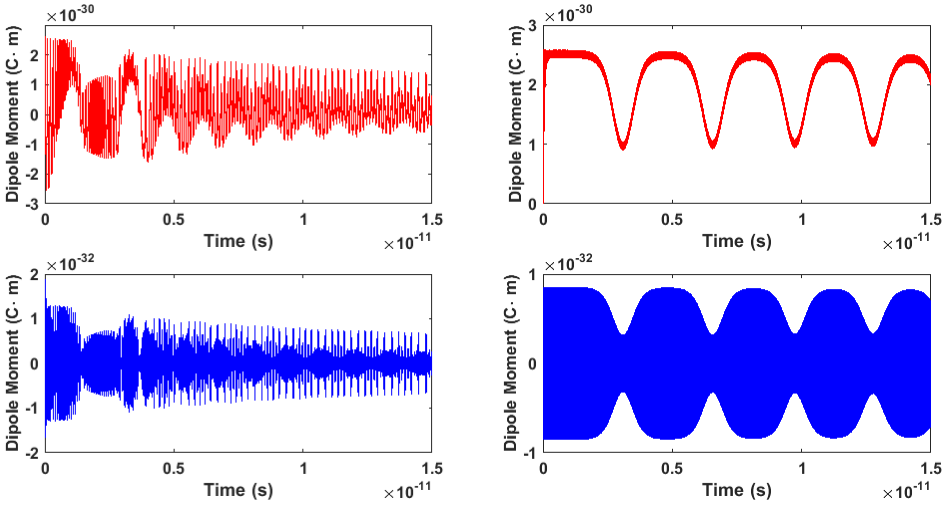

Fig. 6. High-field charge separation (top) and high-field magnetization/c (bottom) computed for low damping, $\gamma = 0.05$ (left) and high damping, $\gamma = 0.2$ (right). Other fixed parameters were $E = 1 \times 10^{10} V/m$ and $I_{\perp} / I_{//} = 1000$.

Finally, the dependences of magneto-electric rectification and magnetization on intensity were calculated for representative values of the librational frequency ω_{ϕ} of the electron in the reference frame of the molecule, using the classical model. The results are summarized in Fig. 7. Three different values of ω_{ϕ} / ω_0 were considered to illustrate the effect of magnetic torque on the enhancement of M-E effects. A complication of these simulations was that the model destabilized when ω_{ϕ} was varied widely for a fixed value of $r_A(0)$. This problem was addressed by running stable computations with initial tether positions that were scaled according to $r_A(0) \propto \sqrt{1/\omega_{\phi}}$ and then correcting the results with the inverse factor (to which the steady-state moment is proportional). Because our simulations assume step-function excitation, steady-state response (at long times) also reflects a saturation limit that must be avoided to discern the proportionality of response with intensity. Below saturation, the values of all the moments were therefore determined at elapsed times of $\tau = 1/\omega_0 \omega_{\phi}$ to cancel the effect of libration frequency on the theoretical torque completion time, which is $\tau_{theor} = 4\omega_{\phi} / \omega_c \omega_0$ (see [13]). This provided appropriate scaling in time for different libration frequencies.

From the plots in Fig. 7, it is readily seen that the square of the rectification moment is quadratic with respect to photon number (or intensity) until it reaches a plateau (saturation level). There its value is constant and equals the dipole moment calculated from the steady-state tether position. The squared magnetization has a cubic dependence on input intensity in the classical picture and displays a strong dependence on the rotation frequency similar to that in the rectification curves. In the next section it is shown that a quantum mechanical formulation of these dynamics predicts the same behavior, with the exception that magnetization undergoes quadratic growth at low intensities before reaching the cubic regime and saturation of the rectification moment is determined by the transition dipole moment rather than a mechanical tether position.

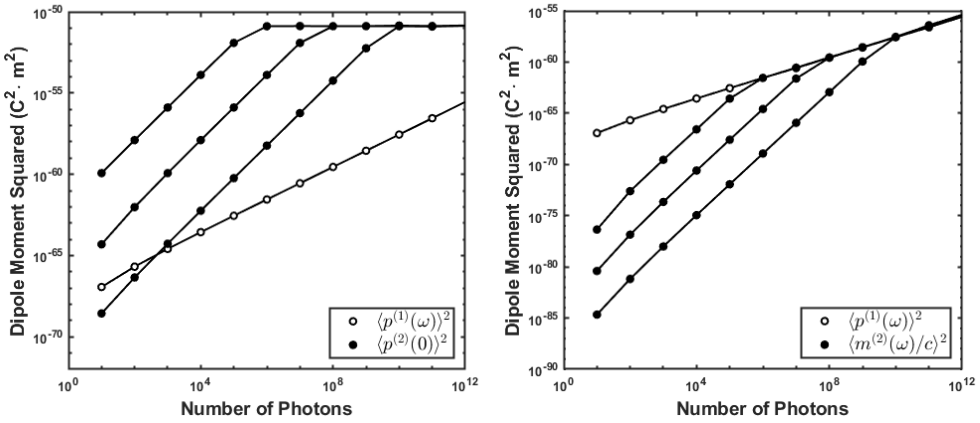

(a) (b)

Fig. 7. (a) Squared magnitudes of the magneto-electric rectification dipole moment (filled circles) compared to the linear ED moment (open circles) as a function of photon number. The ED moment is proportional to input photon number (or intensity) and determines Rayleigh scattering intensity. The nonlinear rectification moment is plotted as three curves with filled circles corresponding to different ratios of $\omega_\phi / \omega_0 = 10^{-7}$, 10^{-5}, 10^{-3} (left to right). (b) Squared magnitudes of the induced magnetic moment (proportional to the magnetic scattering intensity) versus number of incident photons for ratios of $\omega_\phi / \omega_0 = 10^{-7}$, 10^{-5}, 10^{-3} (left to right). In both (a) and (b) filled circles are nonlinear moments whereas open circles are linear ED moments shown for the purpose of direct comparison.

3. Quantum model

A quantum theory equivalent to the model of Section 2 may be formulated for a homonuclear diatomic molecule (symmetric top) with a 1-photon electric dipole (*ED*) resonance at frequency ω_0. The quantization axis lies along the axis of the molecule [23]. Without loss of generality the electric field at frequency ω may also be assumed to point in this direction (i.e. along $\hat{x}$) and to propagate along $\hat{z}$. The ground electronic state is taken to be $^1\Sigma_g^+$, the excited state $^1\Pi_u$, and orbital angular momentum is specified by the eigenvalue of L and its projection m_l (or Λ) on the axis (see [23]). Following an earlier analysis [13], uncoupled electronic states are denoted by $|aLm_l\rangle$ with $a = 1, 2$ specifying the principal quantum number. The basis states support an *ED* transition from $L = 0$ to $L = 1$ followed by a magnetic dipole (*MD)* transition from $m_l = 0$ to $m_l = \pm 1$. The four states $|100\rangle, |210\rangle, |21\text{-}1\rangle$ and $|211\rangle$ comprise the electronic basis. For pedagogical purposes, the basis state $|211\rangle$ is at first omitted from the analysis. This has the benefit of reducing the dimensionality of the eigenvalue problem from 4×4 to 3×3. This allows an analytic method of solution to be illustrated while introducing only a small error in the calculated rectification polarization. Numerically exact results are provided at the end of the paper by reinserting state $|211\rangle$ into the basis set and re-calculating the dipole moments.

In the pedagogical 3-state model, molecular rotational states are written $|Om_o\rangle$ and comprise only $|00\rangle$, $|10\rangle$ and $|11\rangle$ (see Appendix A of [13]). The optical field is assumed to

be a single-mode Fock state $|n\rangle$. The molecule-field states therefore form the uncoupled product states $|1\rangle \circ |100\rangle|00\rangle|n\rangle, |2\rangle \circ |210\rangle|10\rangle|n-1\rangle$, and $|3\rangle \circ |21-1\rangle|11\rangle|n\rangle$. These are eigenstates of the molecule-field Hamiltonian

$$\hat{H}_{mf} = \hat{H}_{mol} + \hat{H}_{field} = (\hbar\omega_0/2)\hat{\sigma}_z + \hat{O}^2/2I + \hbar\omega\hat{a}^+\hat{a}^-, \tag{3.1}$$

with eigenenergies $E_i (i = 1,2,3)$ defined by $\hat{H}_{mf}|i\rangle = E_i|i\rangle$. $\hat{O}^2/2I$ designates kinetic energy of molecular rotation perpendicular to the internuclear axis with moment of inertia *I*. Basis state energies are:

$$E_1 = -\frac{\hbar\omega_0}{2} + n\hbar\omega, \tag{3.2}$$

$$E_2 = E_1 + \hbar\Delta = \frac{\hbar\omega_0}{2} + (n-1)\hbar\omega, \tag{3.3}$$

$$E_3 = E_2 - \hbar\Delta + \hbar\omega_\varphi = -\frac{\hbar\omega_0}{2} + n\hbar\omega. \tag{3.4}$$

In Eq. (3.1) above, $\hat{\sigma}_z$ is a Pauli spin operator. $\hat{a}^+$ and $\hat{a}^-$ are raising and lowering operators of the single mode field respectively. The sign of the first term on the right of Eq. (3.4) reflects the fact that state 3 has rotational energy $\hbar\omega_\varphi \equiv \hbar^2/I$ but no internal electronic kinetic energy (i.e. no electronic excitation). As depicted in Fig. 8, and discussed further below, this is the terminal state of an allowed 2-photon interaction that terminates in a rotationally-excited ground state sublevel as the result of magnetic torque.

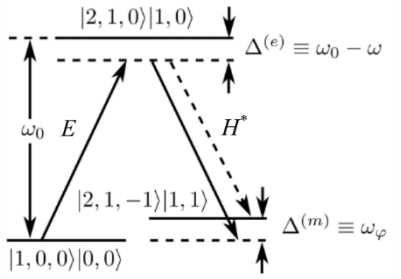

Fig. 8. Energy levels of the molecular model showing the 2-photon transition (solid arrows) driven by the optical E and H^* fields The dashed downward arrow depicts a magnetic de-excitation channel that becomes an option if the excitation bandwidth exceeds ω_ϕ.

Next, the rotating-wave approximation (RWA) is made for both the electric and magnetic field interactions. This is consistent with a small 1-photon detuning $\Delta = \omega_0 - \omega$, and also with a small 2-photon detuning (ω_ϕ) of the H^*E process ($\omega_\phi << \omega$). Next, the magnetic interaction $\hat{H}^{(m)}_{\text{int}} = -\mu^{(m)}_{\hat{O}} \cdot (\bar{L} \times \bar{B}/\hbar)$, which includes torque by the optical magnetic field on the orbital angular momentum, is introduced [13]. The quantized form of this interaction Hamiltonian is:

$$\hat{H}_{\text{int}} = \hat{H}^{(e)}_{\text{int}} + \hat{H}^{(m)}_{\text{int}} = \hbar g(\hat{\sigma}^+\hat{a}^- + h.c.) + (\hbar f \hat{L}'_- \hat{O}'_+ \hat{a}^+ + h.c.), \tag{3.5}$$

Primes on the orbital ($\hat{L}'_{\pm} \equiv \hat{L}_{\pm}/\hbar$) and rotational angular momentum operators ($\hat{O}'_{\pm} \equiv \hat{O}_{\pm}/\hbar$) indicate division by $\hbar$. The prefactors are $\hbar g \equiv -\mu_0^{(e)}\xi$ and $\hbar f \equiv -\mu_{eff}^{(m)}\xi/c$, where $\mu_{eff} \equiv i\left(2\omega_0/\omega_c\right)\mu_0^{(m)}$ is the effective magnetic moment; $\xi \equiv \sqrt{\hbar\omega/2\varepsilon_0 V}$ is the electric field per photon. $\hat{H}_{\text{int}}^{(m)}$ is shown in the appendix to be PT-symmetric although it is Hermitian. The full Hamiltonian is $\hat{H} = \hat{H}_{mol} + \hat{H}_{field} + \hat{H}_{\text{int}}$, and the corresponding eigenvalue equation is $\hat{H}\left|D\right\rangle = E_D\left|D\right\rangle$ in the uncoupled basis, with

$$\begin{pmatrix} E_3 & 2\hbar f\sqrt{n} & 0 \\ 2\hbar f^{*}\sqrt{n} & E_2 & \hbar g\sqrt{n} \\ 0 & \hbar g^{*}\sqrt{n} & E_1 \end{pmatrix}\begin{pmatrix} c_i \\ b_i \\ a_i \end{pmatrix} = E_{Di}\begin{pmatrix} c_i \\ b_i \\ a_i \end{pmatrix}. \tag{3.6}$$

The secular equation

$$\left(H - E_{Di}I\right)\left|D_i(n)\right\rangle = 0, \tag{3.7}$$

may be solved by a "dressed" state approach [24], which in this case will determine "doubly-dressed" eigenstates of the form

$$\left|D_i(n)\right\rangle = a_i\left|100\right\rangle\left|00\right\rangle\left|n\right\rangle + b_i\left|210\right\rangle\left|10\right\rangle\left|n-1\right\rangle + c_i\left|21-1\right\rangle\left|11\right\rangle\left|n\right\rangle, \tag{3.8}$$

together with their eigenenergies E_{Di}. These energy levels are illustrated in Fig. 9, together with dipole moments between their components that are allowed in the dressed state picture by the usual selection rules for ED and MD transitions.

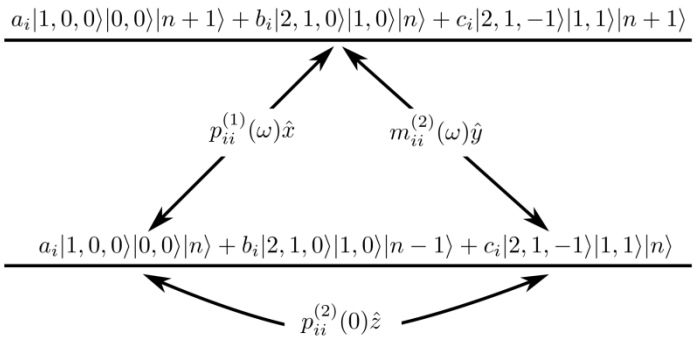

Fig. 9. Diagram of three dipole moments formed by strong excitation of a nominally 2-level molecule during a 2-photon EB^{*} process. $p^{(1)}(\omega)\hat{x}$ is the linear *ED* polarization along the quantization axis. $p^{(2)}(0)\hat{z}$ and $m^{(2)}(\omega)\hat{y}$ are nonlinear rectification and magnetization moments oriented along $\hat{z}$ and $\hat{y}$ respectively.

The eigenvalue problem of the 3-state model can be solved by diagonalization. The results can be found in [13], illustrating an analytic approach (that is approximate) to this problem. The admixed components of the dressed states mediating the electric dipole transition moment, the rectification moment, and the magnetic moment are all shown in Fig. 9. Numerical plots of $\left\langle \hat{p}^{(1)}(\omega)\right\rangle$ and $\left\langle \hat{p}_z^{(2)}(0)\right\rangle$ are presented next in Fig. 10 as a function of

pump photon number, or intensity, for several values of the rotation frequency of the molecule. The results shown were obtained by including the fourth state of the full basis in which the dressed states become

$$\left| D_i(n) \right\rangle = a_i \left| 100 \right\rangle \left| 00 \right\rangle \left| n \right\rangle + b_i \left| 210 \right\rangle \left| 10 \right\rangle \left| n-1 \right\rangle + c_i \left| 21-1 \right\rangle \left| 11 \right\rangle \left| n \right\rangle + d_i \left| 211 \right\rangle \left| 11 \right\rangle \left| n \right\rangle, \tag{3.9}$$

and the index *j* runs from 1 to 4. The rectification moment may be written as

$$\left| \left\langle \hat{p}^{(2)}(0) \right\rangle \right| = \sqrt{2}\mu^{(e)} \left[\sum_{j=1}^{4} \left| \left(a_j c_j^* + a_j d_j^* \right) + c.c. \right|^2 \right]^{1/2}. \tag{3.10}$$

The upper limit of $\left\langle \hat{p}_z^{(2)}(0) \right\rangle$ in Fig. 10 is determined by the Bohr radius in this hydrogenic model to be $\sqrt{2} e a_0$ [21]. The induced magnetic moment $\left\langle \hat{m}(\omega) \right\rangle$ on the transition between states 2 and 3 (and between states 2 and 4) was calculated from the expression

$$\left| \left\langle \hat{m}(\omega) \right\rangle \right| = 2\mu_{eff}^{(m)} \left[\sum_{j=1}^{4} (a_j b_j^* + c.c.)^2 + (a_j d_j^* + c.c.)^2 \right]^{1/2}. \tag{3.11}$$

Results for $\left(\left\langle \hat{m}(\omega) \right\rangle / c \right)^2$ are plotted in Fig. 10 in the same 4-state basis.

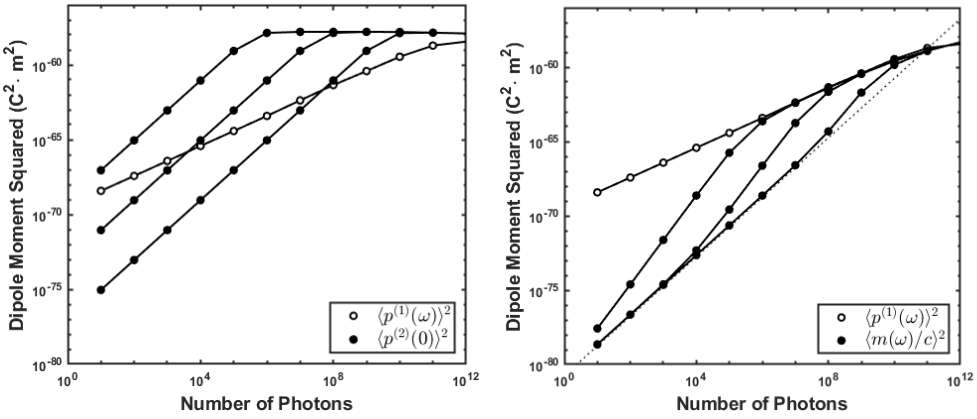

(a) (b)

Fig. 10. (a) Squared quantum ED moment $p^{(1)}(\omega)$ (open circles) and the nonlinear rectification moment $p^{(2)}(0)$ (filled circles) versus incident photon number in three curves reflecting different ratios of the rotational and resonance frequencies given by $\omega_\phi / \omega_0 = 10^{-7}$, 10^{-5}, 10^{-3} (left to right). (b) Squared quantum ED moment $p^{(1)}(\omega)$ (open circles) and the MD moment plotted as $m(\omega)/c$ versus photon number for the same three values of the rotation frequency ω_ϕ. In both (a) and (b) filled circles are nonlinear moments whereas open circles are linear ED moments shown for direct comparison.

4. Results and conclusions

The classical molecular model developed in Section 2 exhibited nonlinear behavior quite distinct from the elementary Drude-Lorentz model [19] as the direct result of including the

Lorentz force and magnetic torque. The appearance of two enhanced magneto-electric effects driven by the optical fields was in excellent agreement with the more detailed results of quantum theory in Section 3. In particular both analyses predicted magneto-electric rectification, which is of primary interest in this paper, and its enhancement by magnetic torque when the ratio of transverse to parallel moments of inertia, namely $I_{\perp} / I_{//}$, is large. In fact the longitudinal ED moment in M-E rectification can be enhanced to the degree that it exceeds the linear ED moment driven by the incident electric field (over a limited intensity range). For values of the inertial ratio exceeding the inverse fine structure constant ($I_{\perp} / I_{//} > (1/\alpha)$) the calculations also revealed that optical magnetization can be as large as the linear electric polarization under non-relativistic conditions. The physical mechanism for enhancement of M-E effects is illustrated in Fig. 12, where the initial area enclosed by charge libration in a molecule is seen to grow as the result of torque dynamics which convert orbital angular momentum to rotational angular momentum (see also [13]). For both rectification and magnetization the requirement for full enhancement of either the rectification or the magnetization is that $I_{\perp} / I_{//} > (1/\alpha)$.

Regarding temporal behavior, simulations showed that the time required to reach steady-state behavior is strongly affected by optical field strength, librational damping rate and the $I_{\perp} / I_{//}$ ratio of the molecular model. High field strengths speeded up torque dynamics and the appearance of M-E rectification. A small damping rate resulted in under-damped Rabi oscillations that persisted in time without much effect on the amplitude of response. High $I_{\perp} / I_{//}$ ratios shortened the time required to reach maximum charge separation or maximum magnetization by making magnetic torque more effective. In high fields, instabilities that were affected by changes in the librational damping parameter appeared.

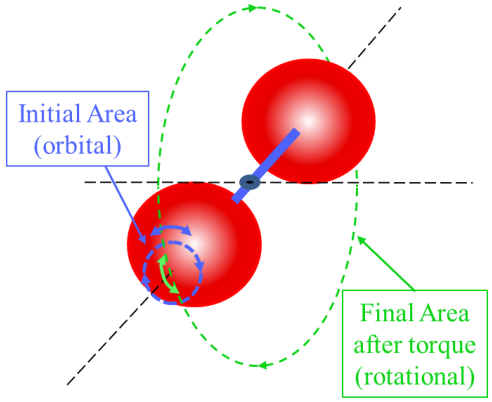

Fig. 12. Magnetic torque mediates a rotation of the axis about which there is electron angular momentum in a molecule. The axis rotation causes a transfer of orbital angular momentum to rotational (librational) angular momentum, thereby enlarging the area enclosed by circular electron motion.

Quantum theory presented in Section 3 closely paralleled the classical model, predicting the nonlinear electric polarization $p^{(2)}(0)$ to be quadratic with respect to the input field amplitude (linear with respect to the number of photons) at all intensities below a well-defined saturation point where it reaches a constant value given by the ED transition moment in the hydrogenic model. The nonlinear magnetic moment $m(\omega)$ was similarly quadratic with respect to the input fields (linear with respect to the number of photons) at low intensities, but underwent an interval of cubic growth before saturating at a value equal to the induced ED

moment $p^{(1)}(\omega)$ at high intensities. Importantly, the downward magnetic transition in Fig. 8 which changes the principal quantum number and produces enhanced magnetic response was found to be an allowed process when torque is considered. The quadratic portion of the magnetization response is a purely quantum mechanical feature of the predictions that relies on the formation of a non-radiative, 2-photon coherent state [13]. Cubic response of the magnetic moment on the other hand is driven by the field combination $M \propto EH^{*}E$. The potentially competitive process $M \propto HH^{*}E$ is forbidden under inversion symmetry [25]. In the saturation regime, the magnetization maintained a linear dependence on the input intensity, equalling the (linear) electric polarization responsible for Rayleigh scattering. Physically, induced magnetization cannot exceed the electric polarization since the optical magnetic field can only deflect motion initiated by the electric field. Ultimately both the ED and MD moments cease to grow when the ionization threshold is reached (on the far right of Figs. 10 and 11).

The substantial agreement obtained between the classical and quantum approaches of this paper is evident from a comparison of Figs. 7 and 10. This confirms that strong magneto-electric rectification (and magnetization) at the molecular level may thus be accounted for by the torque-mediated transfer of orbital to rotational angular momentum. The enhancement mechanism is due to an exchange of angular momentum in a fashion reminiscent of the Einstein-deHaas effect in which spin angular momentum is converted to macroscopic rotation of an unmagnetized body [10]. Yet spin plays no role in the theory presented here. Due to P-T symmetry of the magnetic torque Hamiltonian, M-E rectification is also predicted to be universally allowed in spinless dielectric systems at the molecular level.

The intensity I_{sat} at which the static M-E polarization saturates depends on structural aspects of the individual molecules, especially the ratio of moments of inertia determining the excited state and rotational (librational) frequencies. The rotational frequency governs the 2-photon detuning of the process, so it is not surprising that the intensity I_{sat} at which maximum response is attained varies in proportion to the rotation/libration frequency W_j. In molecular liquids the rotation frequency is given by $\omega_{\varphi} = \hbar / I$, so an inverse dependence on moment of inertia is expected. In solids there is no well-defined moment of inertia at the molecular level. Nevertheless, librational frequencies associated with localized optical centers are well-defined excitations that may be represented by a dominant frequency W_j or a distribution of librational frequencies. Hence the intensity requirement for saturated M-E rectification (and magnetization) can be expected to drop as such characteristic frequencies are reduced in liquids and solids alike. Other structural and chemical aspects of the medium, such as the strength of the transition dipole and the orientational damping constant affect the separation of charge as well (as indicated by Figs. 2-4). The present work therefore offers concrete guidelines with which to optimize materials for magneto-electric rectification. These results augment a complementary analysis of off-diagonal elements of the third order electric susceptibility tensor which provides design rules to optimize M-E materials [25] but in addition the results presented here permit the prediction of temporal dynamics.

Appendix A. Parity-time symmetry of the magnetic interaction Hamiltonian

In this section the symmetry properties of the quantized magneto-electric Hamiltonian are examined under reversal of time and space coordinates. It is shown that although neither parity nor time-reversal symmetry is obeyed on an individual basis, the combination of time- and space inversion is a valid dynamic symmetry for M-E interactions. Thus systems that evolve according to this Hamiltonian are parity-time (P-T) symmetric.

The magnetic portion of the interaction Hamiltonian in Eq. (3.5) that governs the second step of magneto-electric interactions at the molecular level is

$$\hat{H}_{\text{int}}^{(m)} = (\hbar f \hat{L}'_{-} \hat{O}'_{+} \hat{a}^{+} + h.c.)\,. \tag{A.1}$$

As shown below, the magnetic dynamics described this Hamiltonian obey parity (P) and time (T) reversal symmetry only in combination. To establish this result, the effects of applying P and T symmetries to the individual operators in $\hat{H}_{\text{int}}^{(m)}$ are analyzed and then their combined effects are determined.

The operators $\hat{L}$ and $\hat{O}$, governing orbital and rotational angular momentum respectively, transform identically under time reversal and spatial inversion. Hence it is sufficient to analyze the transformation properties of only one of them, say $\hat{L} = \hat{r} \times \hat{p}$, using its representation in terms of the real space coordinate r and the linear momentum $p = dr / dt$ of a charge in motion. Now the motion variables themselves obey the transformations $\hat{P}(\hat{r}) = -\hat{r}$; $\hat{T}(\hat{r}) = \hat{r}$ and $\hat{P}(\hat{p}) = -\hat{p}$; $\hat{T}(\hat{p}) = -\hat{p}$. Consequently it is straightforward to determine the effects of applying parity and time-reversal operators to an angular momentum operator.

$$\begin{aligned}
\hat{P}(\hat{L}_{\pm}) &= \hat{P}\left\{\hat{L}_x \pm i\hat{L}_y\right\} \\
&= \hat{P}\left\{(\hat{y}\hat{p}_z - \hat{z}\hat{p}_y) \pm i(\hat{z}\hat{p}_x - \hat{x}\hat{p}_z)\right\} \\
&= \left\{[(-\hat{y})(-\hat{p}_z) - (-\hat{z})(-\hat{p}_y)] \pm i[(-\hat{z})(-\hat{p}_x) - (-\hat{z})(-\hat{p}_z)]\right\} \\
&= -\hat{L}_{\pm}
\end{aligned} \tag{A.2}$$

$$\begin{aligned}
\hat{T}(\hat{L}_{\pm}) &= \hat{T}\left\{\hat{L}_x \pm i\hat{L}_y\right\} \\
&= \hat{T}\left\{(\hat{y}\hat{p}_z - \hat{z}\hat{p}_y) \pm i(\hat{z}\hat{p}_x - \hat{x}\hat{p}_z)\right\} \\
&= \left\{[(\hat{y})(-\hat{p}_z) - (\hat{z})(-\hat{p}_y)] \pm i[(\hat{z})(-\hat{p}_x) - (\hat{z})(-\hat{p}_z)]\right\} \\
&= -\hat{L}_{\mp}
\end{aligned} \tag{A.3}$$

Similarly, the optical field raising and lowering operators may be represented by the canonical variables q and p according to $\hat{a}^{\mp} = \sqrt{\frac{\omega}{2\hbar}}\left(\hat{q} \pm i\frac{\hat{p}}{\omega}\right)$. Hence the field transformations are similarly determined by space and momentum properties.

$$\begin{aligned}
\hat{P}\left\{\hat{a}^{\mp}\right\} &= \hat{P}\left\{\sqrt{\frac{\omega}{2\hbar}}\left(\hat{q} \pm i\frac{\hat{p}}{\omega}\right)\right\} \\
&= \left\{\sqrt{\frac{\omega}{2\hbar}}\left((-\hat{q}) \pm i\frac{(-\hat{p})}{\omega}\right)\right\} \\
&= -\hat{a}^{\mp} \neq \hat{a}^{\mp}
\end{aligned} \tag{A.4}$$

$$\begin{aligned}\hat{T}\left\{\hat{a}^{\mp}\right\} &= \hat{T}\left\{\sqrt{\frac{\omega}{2\hbar}}\left(\hat{q} \pm i\frac{\hat{p}}{\omega}\right)\right\} \\ &= \left\{\sqrt{\frac{\omega}{2\hbar}}\left(\hat{q} \mp i\frac{\hat{p}}{\omega}\right)\right\} \\ &= \left\{\hat{a}^{\mp}\right\}^{+} \neq \hat{a}^{\mp}\end{aligned} \tag{A.5}$$

Combining the results of Eqs. (A.2-A.5), the magnetic part of the Hamiltonian is found to transform as follows:

$$\begin{aligned}\hat{P}(\hat{H}_{\text{int}}^{(m)}) &= \hat{P}(\hbar f\hat{L}'_{-}\hat{O}'_{+}\hat{a}^{+} + \hbar f^{*}\hat{L}'_{+}\hat{O}'_{-}\hat{a}^{-}) \\ &= \hbar f(-\hat{L}'_{-})(-\hat{O}'_{+})(-\hat{a}^{+}) + \hbar f^{*}(-\hat{L}'_{+})(-\hat{O}'_{-})(-\hat{a}^{-}) \\ &= -\hat{H}_{\text{int}}^{(m)} \neq \hat{H}_{\text{int}}^{(m)}\end{aligned} \tag{A.6}$$

$$\begin{aligned}\hat{T}(\hat{H}_{\text{int}}^{(m)}) &= \hat{T}(\hbar f\hat{L}'_{-}\hat{O}'_{+}\hat{a}^{+} + \hbar f^{*}\hat{L}'_{+}\hat{O}'_{-}\hat{a}^{-}) \\ &= \hbar f(-\hat{L}'_{+})(-\hat{O}'_{-})(\hat{a}^{-}) + \hbar f^{*}(-\hat{L}'_{-})(-\hat{O}'_{+})(\hat{a}^{+}) \\ &= -\hat{H}_{\text{int}}^{(m)} \neq \hat{H}_{\text{int}}^{(m)}\end{aligned} \tag{A.7}$$

$$\begin{aligned}\hat{P}\hat{T}(\hat{H}_{\text{int}}^{(m)}) &= \hat{P}\hat{T}(\hbar f\hat{L}'_{-}\hat{O}'_{+}\hat{a}^{+} + \hbar f^{*}\hat{L}'_{+}\hat{O}'_{-}\hat{a}^{-}) \\ &= \hbar f(-)^{2}\hat{L}'_{+}(-)^{2}\hat{O}'_{-})(-\hat{a}^{-}) + \hbar f^{*}(-)^{2}\hat{L}'_{-})(-)^{2}\hat{O}'_{+})(-\hat{a}^{+}) \\ &= \hat{H}_{\text{int}}^{(m)}\end{aligned} \tag{A.8}$$

According to (A.6) and (A.7), the magnetic interaction Hamiltonian does not obey either spatial inversion or time reversal symmetry separately. However in Eq. (A.8) it is invariant under the combined symmetry operations of parity and time reversal.

Funding

Air Force Office of Scientific Research (AFOSR) (FA9550_12_1_0119) and (FA9550_14_1_0040).

Acknowledgments

This research was supported by the MURI Center for Dynamic Magneto-optics (AFOSR FA9550-14-1-0040). E.F.C.D. gratefully acknowledges an NSF Graduate Research Fellowship and a University of Michigan Rackham Merit Fellowship.